PHYSICAL REVIEW E **74**, 010602(R) (2006)

Observation of a low-viscosity interface between immiscible polymer layers

Xuesong Hu,[1] Zhang Jiang,[2] Suresh Narayanan,[3] Xuesong Jiao,[4] Alec R. Sandy,[3] Sunil K. Sinha,[2] Laurence B. Lurio,[4] and Jyotsana Lal[1]

[1]*Intense Pulsed Neutron Source, Argonne National Laboratory, Argonne, Illinois 60439, USA*

[2]*Department of Physics, University of California, San Diego, La Jolla, California 92093, USA*

[3]*Advanced Photon Source, Argonne National Laboratory, Argonne, Illinois 60439, USA*

[4]*Department of Physics, Northern Illinois University, DeKalb, Illinois 60115, USA*

(Received 18 January 2006; revised manuscript received 7 June 2006; published 19 July 2006)

X-ray photon correlation spectroscopy was employed in a surface standing wave geometry in order to resolve the thermally driven in-plane dynamics at both the surface/vacuum (top) and polymer/polymer (bottom) interfaces of a thin polystyrene (PS) film on top of Poly(4-bromo styrene) (PBrS) and supported on a Si substrate. The top vacuum interface shows two relaxation modes: one fast and one slow, while the buried polymer-polymer interface shows a single slow mode. The slow mode of the top interface is similar in magnitude and wave vector dependence to the single mode of the buried interface. The dynamics are consistent with a low-viscosity mixed layer between the PS and PBrS and coupling of the capillary wave fluctuations between this layer and the PS.

DOI: 10.1103/PhysRevE.74.010602 PACS number(s): 68.03.Kn, 82.35.Gh, 61.10.Eq, 83.80.Sg

Polymer/polymer interfaces play an important role in the mechanical toughness of polymer blends, adhesion properties in coatings, and co-extrusion of polymers. It has been reported that immiscible polymer blends can have viscosities lower than either of their components [1] and recent multilayer co-extrusion experiments indicate that the lower viscosity is due to interfacial slip [2]. Normally, interfaces between immiscible polymers exhibit poor adhesion [3] and this is attributed to weak entanglements between dissimilar polymers at an interface [4]. Dissipation within the interfacial regions can only be indirectly studied with bulk rheological measurements. Most results are in qualitative agreement with theories [4–7] that predict fewer chain entanglements near the interface between two immiscible polymers and thus a small interface width with lower viscosity. The lower viscosity at the interface explains slip on application of shear; however, existing theories overpredict the slip effect [2].

Here we report on the development of a technique, employing x-ray photon correlation spectroscopy [8] in a surface standing wave geometry [9], which provides a way to resolve the dynamics at buried polymer-polymer interface at nanoscale resolution both parallel and perpendicular to the interface. The position of the maxima of an x-ray standing wave incident on the surface of a polymer is moved to different positions in a film by changing the incident angle. This allows scattering to be selectively obtained from either the surface or buried interface of a polymer film in a single bilayer. If the exciting wave is partially coherent, one can then selectively measure dynamics from each region using x-ray photon correlation spectroscopy (XPCS). The nanometer scale spatial resolution provides a significant advance in knowledge over multilayer coextrusion methods, and can provide tests of theoretical models which address hydrodynamic modes of viscoelastic polymer films and interface slip [10,11]. This method should also find wide applicability to the emerging field of microfluidics [12–14]. The XPCS technique described here can be refined to study driven flows of complex fluids in nanofluidic and microfluidic devices where one could manipulate fluids exploiting boundary effects if they were understood better on microscopic scales [15].

The samples consist of a bilayer of polystyrene (PS) on top of poly(4-bromo styrene) (PBrS) supported on a single crystal silicon wafer (PS/PBrS/Si). The silicon wafers were cleaved into 15 mm squares, cleaned in sulfuric acid, and then stripped of their oxide layer using HF. The polystyrene (M_W=200 k, M_W/M_n=1.06) was obtained from Polymer Source. The PBrS was obtained by brominating PS (M_W=350 k, M_W/M_n=1.06) [16] resulting in a bromination fraction of x=89%. PBrS was spun cast from toluene solution directly onto the silicon wafers. PS was spun cast onto a glass slide and floated from deionized water onto the PBrS layer. Samples were annealed at 180 °C in an oil-trapped vacuum of 10^{-3} Torr for 12 h. For a high degree of bromination, the Flory-Huggins interaction parameter χ=0.064 for PS/PBrS at 180 °C and $\chi > \chi_{c,}=1.04\times10^{-3}$ indicates strong incompatibility of our polymers [4,17]. Strongly incompatible polymers only intermix on a segmental scale, hence their interface widths are several nm wide, but remain finite [4,17]. Two bilayer geometries were prepared: 100 nm PS on 100 nm PBrS, and 100 nm PS on 200 nm with PBrS layer. These geometries yielded essentially identical results, so we focus here on the 100 nm PS on 200 nm PBrS system.

The experiments were performed in a grazing incidence geometry [18–22]. The scattering vector defined by $\mathbf{q}=\mathbf{k}_{out}-\mathbf{k}_{in}$ relative to the incident and outgoing x-ray wave vectors, can be decomposed relative to the surface normal, $q_\perp=\mathbf{q}\cdot\hat{\mathbf{n}}$ and $q_\parallel=|\mathbf{q}\times\hat{\mathbf{n}}|$. The critical angle ($\alpha_c$=0.164 ° at E=7.7 keV) for total external reflection for the top layer (PS) is smaller than that for the bottom layer (PBrS, α_c=0.191 °). Data were measured at two incident angles. X-ray incident at θ_{in}=0.14 ° are below the critical angle of the top layer and the intensity of the electric field decays to zero before it reaches the buried polymer–polymer interface. In this case all scattering originates from the vacuum–polymer interface on the top layer. X-ray incident at θ_{in}=0.18 ° are above the critical angle of the top layer but below that of the bottom layer. A standing wave is set up within the film with a node at the top interface, yielding scattering only from the polymer–polymer interface as shown in Fig. 1 [23].

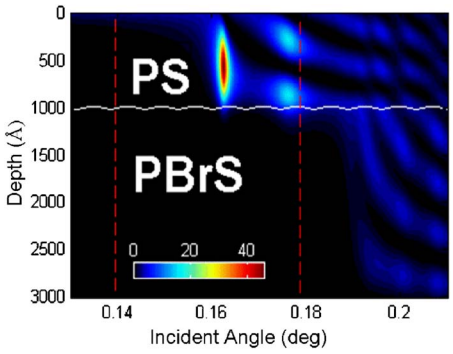

FIG. 1. (Color online) Calculated electric field intensity as a function of depth and incident angle for 100 nm PS/200 nm PBrS/Si at 195 °C.

The diffuse x-ray scattering in this geometry results from capillary wave fluctuations of the interfaces, and the magnitude of the scattering agrees quantitatively with the capillary wave theory [23]. Dynamical properties of the interfaces were characterized via autocorrelation of the surface diffuse x-ray scattering patterns obtained from illuminating the sample with a partially coherent x-ray beam. The scattering was collected on a CCD camera whose pixel size was comparable to the speckle size of the incident x-ray beam [24]. The normalized intensity–intensity autocorrelation function $g_2(q_\parallel,t)$ is related to the normalized intermediate scattering function $f(q_\parallel,t)=S(q_\parallel,t)/S(q_\parallel,0)$ via

$$g_2(q_\parallel,t) = 1 + Af^2(q_\parallel t). \tag{1}$$

Here A is a geometry-dependent optical contrast factor and $S(q_\parallel,t)$ is the dynamic structure factor. For a viscous fluid that exhibits overdamped modes, the intermediate scattering function can often be expressed as a sum over exponentials [25],

$$f(q_\parallel,t) = \sum_i a_i \exp(-t/\tau_i). \tag{2}$$

Here the τ_ι are relaxation times and a_i their amplitudes, with $\Sigma_i a_i = 1$.

Autocorrelation functions, $g_2(t)$, measured at $q_\parallel = 4.3\times10^{-3}$ nm^{-1} from a 100 nm PS/200 nm PBrS/Si bilayer are shown at 176 °C and 206 °C in Figs. 2(b) and 2(d). For comparison, autocorrelation functions measured from an equivalent thickness homolayer film of PS is shown in Figs. 2(a) and 2(c). The PS homolayer is well described by an exponential relaxation of the form $f(q_\parallel,t)=\exp(-t/\tau)$. In the bilayer film, the PS/vacuum (top) interface shows two distinct decay modes, while the PS/PBrS (bottom) interface shows only a single clearly resolved mode. The autocorrelation function of the bottom interface was fit to a single exponential form, while the top interface was fit to the form $f(q_\parallel,t)=a\exp(-t/\tau_1)+(1-a)\exp(-t/\tau_2)$. These fits are shown as the solid lines on top of the data in Fig. 2. The presence of two modes demonstrates that there is coupling between the top and bottom interface due to hydrodynamic flows throughout the film. It is possible to observe this coupling since the thickness, h, of the bilayer is much smaller than the inverse in-plane wave vector $q_\parallel^{-1}$ of the measurement. In Fig. 3 the relaxation times extracted from the measured data are displayed as a function of the wave vector, along with models for the dependence of the relaxation times on the wave vector which will be described in detail below. The corresponding relaxation times for a PS homolayer is also shown for reference. The bilayer τ_1's are faster than the relaxation times for the corresponding PS homolayer and the $q_\parallel$ dependence is weaker. The bilayer relaxation times τ_2 and τ are nearly identical and exhibit a flat $q_\parallel$ dependence.

Measurements were also made on a bilayer with 100 nm PS/100 nm PBrS/Si. The dynamics of the thinner bilayers was identical to the thicker ones. The temperature and thickness dependence of the bottom interface τ's are shown in Fig. 4. The dynamics speed up systematically with tempera-

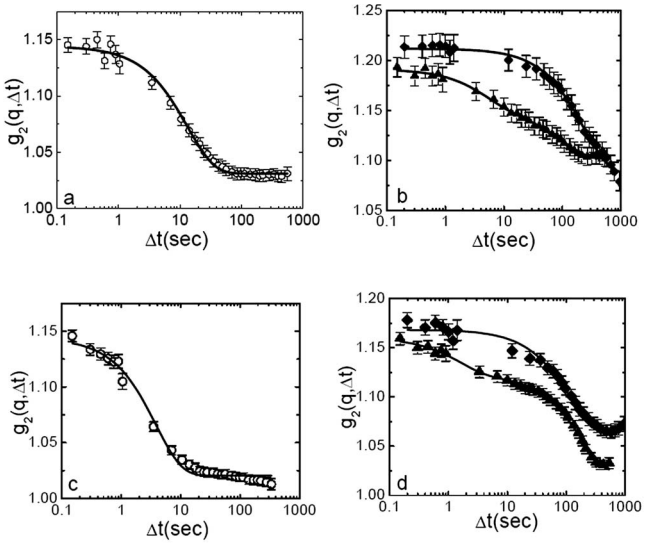

FIG. 2. Autocorrelation functions from single and bilayer films measured at $q_\parallel = 4\times10^{-3}$ nm^{-1}. (a) Single layers films at 176 °C; (○) PS. (b) Bilayer films at 176 °C; (▲) top (◆) bottom. (c) and (d) Single and bilayer films at 205 °C. The solid lines indicate the single and double exponential fits described in the text.

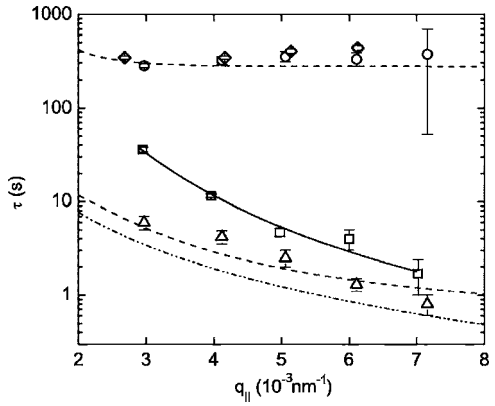

FIG. 3. Measured relaxation times at 195 °C. Bilayer (100 nm PS/200 nm PBrS): (△) τ_1, (O) τ_2, (◇) τ. Corresponding homolayer: (□) 100 nm PS. Theoretical models: (Solid) single layer fit, (dash) low viscosity interface model, (dash-dot-dot) slip model for top PS layer.

ture, as expected, since the viscosity decreases. The time constant is nearly independent of $q_\parallel$ and PBrS thickness. This indicates τ's indeed show dynamics of the interfacial region, as it is insensitive to thickness changes of the bottom PBrS layer.

The dynamics of the homolayer PS film are well described by the relaxation of thermally excited capillary waves [8,26]. In this model, the fluid motion within the PS layer is calculated using the linearized Navier-Stokes equation subject to appropriate boundary conditions. The boundary condition at the bottom of the film is zero velocity relative to the substrate (stick), while the top interface boundary condition is that the viscous stress within the fluid is balanced by the surface tension. The susceptibility of the film to an external force field is then calculated and $f(q_\parallel,t)$ is obtained through the fluctuation dissipation theorem [26]. For overdamped waves on a supported film of height h, fluctuations in height relax with time constants given by

$$\tau = (4\eta h/\gamma)[1 + x^2/2 + \cosh(x)]/[x\sinh(x) - x^2]. \quad (3)$$

Here $x = 2q_\parallel h$, $q_\parallel$ is the wave vector of the fluctuation, η is the viscosity, and γ is the surface tension. This relation has been shown to accurately describe the wave vector dependence of capillary waves on PS films over a wide range of wave vector, thickness, and temperature [8]. Equation (3) adequately describes the homolayer PS films measured in the present study, using values close to the expected surface tension [23], viscosity [27], and film thickness.

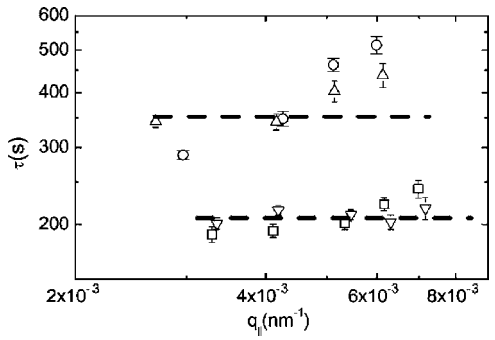

FIG. 4. Temperature and thickness dependence of the relaxation time of the bottom layer: 195 °C: (○) 100 nm PS/100 nm PBrS, (△) 100 nm PS/200 nm PBrS, 225 °C: (▽) 100 nm PS/100 nm PBrS, (□) 100 nm PS/200 nm PBrS.

When the PS film is placed on PBrS instead of Si the fast mode (τ_1) becomes faster than the homolayer relaxation times, as shown in Fig. 3. The change in dynamics is of the same magnitude as would be expected from changing the lower surface boundary condition of the PS film from stick to slip [28], which would change Eq. 3 to $\tau = (4\eta h/\gamma)[x + \sinh(x)]/[x\cosh(x) - x]$. This is shown as the dash-dot-dot line in Fig. 3. The actual data falls intermediate between stick and slip conditions.

We were unable to observe the capillary wave dynamics for the pure PBrS film of thickness 100 nm using XPCS in this experiment as the dynamics of this film were too slow on the time scales for these experiments, presumably owing to its high viscosity. This is also consistent with the known higher value of glass transition temperature T_g for PBrS [29]. Thus in the analysis of the data, the PBrS was considered to be an immobile substrate for the purposes of the boundary conditions applied. This assumption is also justified by the data represented by Fig. 4, where it is seen that the relaxation times are dependent on temperature but *not* on the thickness of the PBrS layer.

The dynamics of the bilayer was modeled as follows. The viscosity of the PS layer is assumed to be uniform throughout the film, and the PBrS layer is assumed immobile at the time scales of the experiment. A thin mixed layer is placed between the PS and PBrS films to account for the interface. Its viscosity is approximated as uniform. A value of 2.6×10^{-3} J/m^2 was used for the interface tension between the mixed layer and the PS film. This was obtained from the magnitude of the surface roughness due to thermally excited, long wavelength capillary modes as measured by static-diffuse x-ray scattering [23]. Static scattering also provides the value of 6.6 nm for the thickness of the mixed layer (assuming the width is 2.35σ, with σ being the Gaussian roughness measured by neutron reflectivity). The linearized Navier-Stokes equation was used to solve for the fluid flow throughout two coupled layers. A stick boundary condition is assumed at the boundary between the mixed layer and the PBrS. At the PS/vacuum interface the surface tension balances the viscous stress. At the interface between the PS and the mixed layer the velocity is continuous and the difference in viscous stress between the two fluids is balanced by the interface tension. The viscoelastic properties of the polymer are taken into account by using a Maxwell-Debye model to represent the viscosity: $\eta(\omega) \approx \eta + i\mu/\omega$. Here μ is a shear modulus and ω is the frequency. For the thick polystyrene film, the effect of the shear modulus is negligible and was ignored. For the thin mixed layer, the addition of shear modulus significantly changes the dynamics [30]. The relaxation times as a function of $q_\parallel$, can be obtained from susceptibility as was done for the PS homolayer. An analytic expression for $\tau(q_\parallel)$ was found using the MATHEMATICA symbolic algebra program, although the explicit form is too long to be reproduced here. The magnitude of the viscosity

and shear modulus of the mixed layer in the resulting equation was then varied using nonlinear least-squares regression to obtain a best fit to the measured experimental relaxation times. This model provides a good fit, shown as the dashed line in Fig. 3, yielding $\mu \sim 18$ N/m^2 and $\eta \sim 327$ Ns/m^2 for the mixed layer. The best fit viscosity is only around 2% of that of the PS layer. Thus, if one only considers the dynamics of the PS fast mode, the mixed layer imbues a finite slip length to the PS/PBrS interface. The dynamics of the slow mode of the top surface, which is nearly identical to the dynamics of the mixed layer, shows almost no dependence on the wave vector. This wave vector dependence cannot be explained by a thin viscous layer, since simple scaling arguments predict a $q_{\|}^{-4}$ dependence for a thin film [31]. However, the inclusion of the shear modulus term produces a flattening of the spectrum. The value of μ obtained from the fits was of the same magnitude of the shear modulus for bulk PS at comparable time scales [32]. Indeed, it has also been found that elasticity effects are required to explain the large q cutoff static roughness due to capillary waves as determined from x-ray scattering [33,34].

While the model described above does give a good fit to the data, it is clear that it approximates the actual interfacial region, since the mixed layer is unlikely to have a uniform viscosity. A surface tension is not applicable over length scales comparable to the thickness of the interface. Nevertheless, the present results provide a significant improvement over previous rheological results. Here we not only imply the existence of slip between PS and PBrS, but we have estimates for the thickness, viscosity, surface tension, and shear modulus of the mixed region. It seems reasonable to speculate that the origin of the low viscosity in the mixed region is similar to the causes of the reduced glass transition at the free surface of PS first observed by Keddie [35], since one might expect that the viscosity above T_g should decrease if T_g decreases. It is significant that PS on silicon does not show a lower viscosity region at the PS/Si interface, indicating that the polymer-polymer interface has a very different character than the polymer-silicon interface. It would be interesting to investigate if thin PS films on top of PBrS show a reduced glass transition temperature, unlike those supported on silicon substrates directly. Finally, we note that experiments on the mobility of gold nanoparticles at the polymer-polymer interface in a bilayer system of PtBA/PtBA [36] have also shown anomalously high mobility. This may be similarly related to a region of reduced viscosity as we have found here.

In summary, using an application of x-ray photon correlation spectroscopy which has been used to identify separately the relaxation modes associated with each interface of a bilayer, together with a viscoelastic theory for the dynamics of a coupled bilayer system, it has been shown that it is not the dynamics of the PBrS underlayer which is relevant, but rather that of a thin low-viscosity interface layer. This somewhat unexpected result is the only model that explains the complete set of q-dependent relaxation times measured here, and provides insights into the rheology of immiscible polymer blends.

We would like to acknowledge helpful discussions with Hyunjung Kim. This work was supported by the U.S. Department of Energy, BES Materials Science, under Contract No. W-31-109-ENG-38 and the NSF Grant No. DMR-020954.

[1] C. D. Han and T. C. Yu, J. Appl. Polym. Sci. **15**, 1163 (1971).
[2] R. Zhao and C. W. Macosko, J. Rheol. **46**(1), 145 (2002).
[3] P. J. Cole *et al.*, Macromolecules **36**, 2808 (2003).
[4] R. Oslanec and H. R. Brown, Macromolecules **36**, 5839 (2003).
[5] H. Furukawa, Phys. Rev. A **40**, 6403 (1989).
[6] P. G. de Gennes, C. R. Seances Acad. Sci., Ser. B **288**, 219 (1979).
[7] F. Brochard-Wyart *et al.*, C. R. Acad. Sci., Ser. II: Mec., Phys., Chim., Sci. Terre Univers **310**, 1169 (1990).
[8] H. Kim *et al.*, Phys. Rev. Lett. **90** 068302 (2003).
[9] L. B. Lurio *et al.*, in *MRS Proceedings No. 790* (Material Research Society, Pittsburgh, 2004).
[10] J. L. Harden and H. Pleiner, Phys. Rev. E **49**, 1411 (1994).
[11] H. Pleiner *et al.*, Europhys. Lett. **7**, 383 (1988).
[12] S. Granick *et al.*, Nature (London) **425**, 467 (2003).
[13] S. Granick, Nat. Mater. **2**, 221 (2003).
[14] N. V. Priezjev and S. M. Troian, Phys. Rev. Lett. **92**, 018302 (2004).
[15] R. Dreyfus *et al.*, Phys. Rev. Lett. **90**, 144505 (2003).
[16] H. Ade *et al.*, Appl. Phys. Lett. **73**, 377 (1998).
[17] B. Guckenbiehl *et al.*, Physica B **198**, 127 (1994).
[18] J. Daillant and A. Gibaud, *X-Ray and Neutron Reflectivity and Scattering: Principles and Applications* (Springer, Heidelberg, 1999).
[19] L. G. Parratt, Phys. Rev. **95**, 359 (1954).
[20] M. Tolan, *X-Ray Scattering from Soft-Matter Thin Films* (Springer, Berlin, 1999).
[21] V. Holy *et al.*, Phys. Rev. B **47**, 15896 (1993).
[22] L. Lurio *et al.*, Macromolecules **36**, 5704 (2003).
[23] X. Hu *et al.*, Eur. Phys. J. E **17**, 353 (2005).
[24] D. Lumma *et al.*, Rev. Sci. Instrum. **71**, 3274 (2000).
[25] D. Lumma *et al.*, Phys. Rev. E **62**, 8258 (2000).
[26] J. Jäckle, J. Phys.: Condens. Matter **10**, 7121 (1998).
[27] D. J. Plazek and V. M. O'Rourke, J. Polym. Sci., Part A-2 **9**, 209 (1971).
[28] S. Herminghaus, Eur. Phys. J. E **8**, 237 (2002).
[29] G. R. Strobl *et al.*, Macromolecules **19**, 2683 (1986).
[30] Z. Jiang *et al.* (unpublished).
[31] *Gouttes, Bulles, Perles et Ondes*, edited by P. G. de Gennes, F. Brochard, and D. Quere (Belin, Paris, 2002).
[32] W. W. Graessley, in *Physical Properties of Polymers*, edited by James E. Mark, A. Eisenberg, W. W. Graessley, L. Mandelkern, E. T. Samulski, J. L. Koenig, and G. D. Wignall (ACS, Washington D.C., 1993).
[33] J. Wang *et al.*, Phys. Rev. Lett. **83**, 564 (1999).
[34] Y. S. Seo *et al.*, Phys. Rev. Lett. **94**, 157802 (2005).
[35] J. L. Keddie *et al.*, Europhys. Lett. **27**, 59 (1994).
[36] Suresh Narayanan *et al.*, Phys. Rev. Lett. **94**, 145504 (2005).